



HAL
open science

On the reliability of direct Rayleigh-wave estimation from multicomponent cross-correlations

Zongbo Xu, T. Dylan Mikesell

► **To cite this version:**

Zongbo Xu, T. Dylan Mikesell. On the reliability of direct Rayleigh-wave estimation from multicomponent cross-correlations. *Geophysical Journal International*, 2017, 210 (3), pp.1388-1393. 10.1093/gji/ggx228 . hal-03919225

HAL Id: hal-03919225

<https://hal.science/hal-03919225>

Submitted on 2 Jan 2023

HAL is a multi-disciplinary open access archive for the deposit and dissemination of scientific research documents, whether they are published or not. The documents may come from teaching and research institutions in France or abroad, or from public or private research centers.

L'archive ouverte pluridisciplinaire **HAL**, est destinée au dépôt et à la diffusion de documents scientifiques de niveau recherche, publiés ou non, émanant des établissements d'enseignement et de recherche français ou étrangers, des laboratoires publics ou privés.

On the reliability of direct Rayleigh-wave estimation from multicomponent cross-correlations

Zongbo Xu and T. Dylan Mikesell

Environmental Seismology Laboratory, Department of Geosciences, Boise State University, Boise, ID, USA. E-mail: zongboxu@u.boisestate.edu

Accepted 2017 May 22. Received 2017 May 19; in original form 2017 March 8

SUMMARY

Seismic interferometry is routinely used to image and characterize underground geology. The vertical component cross-correlations (C_{ZZ}) are often analysed in this process; although one can also use radial component and multicomponent cross-correlations (C_{RR} and C_{ZR} , respectively), which have been shown to provide a more accurate Rayleigh-wave Green's function than C_{ZZ} when sources are unevenly distributed. In this letter, we identify the relationship between the multicomponent cross-correlations (C_{ZR} and C_{RR}) and the Rayleigh-wave Green's functions to show why C_{ZR} and C_{RR} are less sensitive than C_{ZZ} to non-stationary phase source energy. We demonstrate the robustness of C_{RR} with a synthetic seismic noise data example. These results provide a compelling reason as to why C_{RR} should be used to estimate the dispersive characteristics of the direct Rayleigh wave with seismic interferometry when the signal-to-noise ratio is high.

Key words: Seismic interferometry; Surface waves and free oscillations; Wave propagation.

1 INTRODUCTION

Characterizing underground geological structure is important for a variety of applications (e.g. geological hazard assessment, resource exploration, contaminant monitoring, etc.). Nowadays one commonly uses seismic interferometry (SI) to characterize elastic and anelastic properties of the subsurface. Vertical component (Z) data are often used to compute C_{ZZ} cross-correlations (e.g. Shapiro *et al.* 2005), where C_{ZZ} indicates that the vertical channel at both stations is used. From C_{ZZ} , one can estimate an approximate fundamental-mode Rayleigh-wave Green's function (G_{ZZ}) if the seismic sources are distributed evenly (Snieder 2004; Roux *et al.* 2005) or if the wavefield is diffuse (Lobkis & Weaver 2001; Weaver & Lobkis 2006). However, seismic sources are usually not evenly distributed, nor is the wavefield diffuse (Mulargia 2012), and C_{ZZ} leads to a biased estimate of G_{ZZ} (e.g. Halliday & Curtis 2008; Yao & van Der Hilst 2009; Froment *et al.* 2010). One can correct the biased G_{ZZ} using multidimensional deconvolution (Wapenaar *et al.* 2011), the C^3 method (Stehly *et al.* 2008; Froment *et al.* 2011), information about the source distribution (e.g. Yao & van Der Hilst 2009; Nakata *et al.* 2015), or signal processing methods (e.g. Baig *et al.* 2009; Stehly *et al.* 2011; Melo *et al.* 2013). One can also use radial component (R) data to retrieve G_{RR} or a combination of vertical and radial components to retrieve G_{ZR} (e.g. Campillo & Paul 2003; Lin *et al.* 2008; Stehly *et al.* 2009), where the R direction is the in-line direction between the two receivers. van Wijk *et al.* (2011) (empirically) and Haney *et al.* (2012) (theoretically) determined that C_{ZR} and C_{RR} are less sensitive than C_{ZZ} to out-of-line sources,

where out-of-line sources mean the non-stationary phase sources. Stationary-phase sources are defined as sources that constructively interfere to produce the Green's function during correlation; these are sources that have an absolute phase difference less than $\pi/4$ when compared to the real Green's function.

In this letter, we investigate the reliability of cross-correlations affected by an uneven source-energy distribution. Truncating the boundary of sources in seismic interferometry leads to coherent noise (i.e. artefacts or spurious arrivals; e.g. Snieder *et al.* 2006; Mikesell *et al.* 2009). We investigate why C_{ZR} and C_{RR} are more robust than C_{ZZ} to estimate the fundamental-mode Rayleigh wave from a theoretical standpoint and determine why previous studies often find that C_{ZZ} has the largest signal-to-noise ratio (SNR). We first review the relationship between the fundamental-mode Rayleigh-wave Green's function and the cross-correlation function. We then analyse how the source-energy distribution contributes to the cross-correlation and the estimate of the Green's functions. We find that C_{ZR} and C_{RR} attenuate the non-stationary-phase source energy and provide more reliable Rayleigh-wave Green's functions than C_{ZZ} . We further the discussion with a synthetic data example where seismic noise sources are unevenly distributed. We consider how the uneven noise-source distribution affects the virtual shot records and coherent and incoherent noise, as well as the resulting Rayleigh-wave dispersion images. We demonstrate that coherent noise is present prior to the direct-wave arrival, and therefore, this type of noise is often not taken into account when the signal-to-noise ratio of correlations is computed using incoherent noise that arrives after the direct wave.

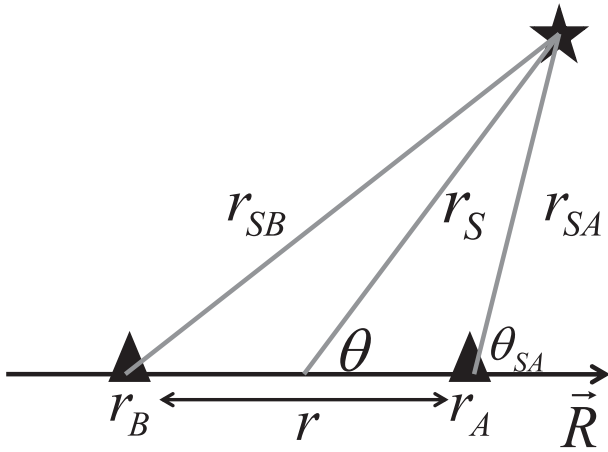


Figure 1. Diagram of the location of a point source (star) and the receivers (triangles). The R direction is parallel to the line linking the two sensors, r_A and r_B .

2 THE GREEN'S FUNCTIONS AND MULTICOMPONENT CROSS-CORRELATIONS

Under the far-field assumption, one can use cross-correlations to approximate the elastic-wave Green's function as

$$G_{im}(r_A, r_B, \omega) - G_{im}^*(r_A, r_B, \omega) \approx -2j\omega \oint_S \frac{1}{\rho c} G_{ip}^*(r_A, r_S, \omega) G_{mp}(r_B, r_S, \omega) dS, \quad (1)$$

where $G_{im}(r_A, r_B, \omega)$ is the Green's function representing the i th component of particle displacement at location r_A due to a point force in the m direction at r_B , the asterisk denotes the complex conjugation, S represents the surface where sources are located, r_S represents the source location, ω is the angular frequency, j is the imaginary unit, ρ is the density and c is the phase velocity (Wapenaar & Fokkema 2006). Here sources are assumed uncorrelated (e.g. Lobkis & Weaver 2001). In a homogeneous medium, and again under the far-field assumption, the vertical component fundamental-mode Rayleigh-wave Green's function can be written as (e.g. Fan & Snieder 2009; Haney *et al.* 2012)

$$G_{ZZ}(r) = \sqrt{\frac{1}{8\pi\omega r/c}} e^{j(\omega r/c + \pi/4)}, \quad (2)$$

where r is the distance between the source and receiver. Regardless of the source direction (i.e. subscript p in eq. 1), if two sensors record in the Z direction, eq. (1) becomes

$$G_{ZZ}(r_A, r_B, \omega) - G_{ZZ}^*(r_A, r_B, \omega) \approx \frac{-j}{4\pi\rho} \oint_S \sqrt{\frac{1}{r_{SA}r_{SB}}} e^{j\omega(r_{SB}-r_{SA})/c} \delta(z) dS, \quad (3)$$

where r_{SA} is the distance between the source r_S and the receiver r_A (Fig. 1), and $\delta(z)$ indicates that all sources are distributed on the $z = 0$ plane, which is the ground surface.

The integrand in eq. (3) is the C_{ZZ} cross-correlation for the source at r_S . When the source is far from the two sensors, $r_{SB} - r_{SA} \approx r \cos(\theta)$ and $r_{SA} \approx r_{SB} \approx r_S$. Because $dS = r_S dz d\theta$, eq. (3) can be written as

$$G_{ZZ}(r_A, r_B, \omega) - G_{ZZ}^*(r_A, r_B, \omega) \approx \frac{-j}{4\pi\rho} \int_0^{2\pi} e^{j\omega r \cos(\theta)/c} d\theta, \quad (4)$$

where the integrand now is the phase of C_{ZZ} for a point source in the θ -direction. Following the same logic, and using

$$G_{RZ}(r) = \frac{H}{V} \sqrt{\frac{1}{8\pi\omega r/c}} e^{j(\omega r/c - \pi/4)}, \quad (5)$$

where H/V is the ratio of the horizontal-to-vertical motion (e.g. Haney *et al.* 2012), we can write

$$G_{ZR}(r_A, r_B, \omega) - G_{ZR}^*(r_A, r_B, \omega) \approx \frac{-j}{4\pi\rho} \frac{H}{V} \int_0^{2\pi} \cos(\theta) e^{j[\omega r \cos(\theta)/c - \pi/2]} d\theta, \quad (6)$$

$$G_{RZ}(r_A, r_B, \omega) - G_{RZ}^*(r_A, r_B, \omega) \approx \frac{-j}{4\pi\rho} \frac{H}{V} \int_0^{2\pi} \cos(\theta) e^{j[\omega r \cos(\theta)/c + \pi/2]} d\theta, \quad (7)$$

$$G_{RR}(r_A, r_B, \omega) - G_{RR}^*(r_A, r_B, \omega) \approx \frac{-j}{4\pi\rho} \left(\frac{H}{V}\right)^2 \int_0^{2\pi} \cos^2(\theta) e^{j\omega r \cos(\theta)/c} d\theta. \quad (8)$$

The integrands in eqs (6)–(8) are C_{ZR} , C_{RZ} and C_{RR} for a point source along the θ azimuth, respectively. Because $G_{RZ}(r_A, r_B, \omega) - G_{RZ}^*(r_A, r_B, \omega) = e^{j\pi} [G_{ZR}(r_A, r_B, \omega) - G_{ZR}^*(r_A, r_B, \omega)] = -[G_{ZR}(r_A, r_B, \omega) - G_{ZR}^*(r_A, r_B, \omega)]$, G_{ZR} possesses the same information as G_{RZ} . The actual source direction (subscript p in eq. 1) is not important; rather the recording direction (subscript m) plays the role of the source during correlation. Thus the Rayleigh waves can be generated by either vertical or horizontal sources (e.g. Nishida *et al.* 2008).

3 THE SIGNIFICANCE OF THE SOURCE ANGLE

The source angle contributes to the three different kinds of cross-correlations, C_{ZZ} , C_{ZR} and C_{RR} , in different ways. One can assess the role of the source angle by considering the integrands of the cross-correlations (e.g. Fan & Snieder 2009). The source distribution area can be divided into two parts: a stationary-phase area (near $\theta = 0, \pi, 2\pi$ in Fig. 2a) and a non-stationary-phase area (the rapid oscillation area in Fig. 2a). The sources in the stationary-phase area are important for retrieving the Green's functions; they contribute significantly to the integral in eq. (1) (Snieder 2004; Snieder *et al.* 2008; Mikesell *et al.* 2012). If the sources are evenly distributed, the integrands of the C_{ZZ} , C_{ZR} and C_{RR} oscillate evenly in the non-stationary-phase area and completely cancel the non-stationary-phase energy in the integral from 0 to 2π . However, we are interested in the sources in the non-stationary-phase area; thus we consider an isolated number of sources in small angular range.

At a constant receiver separation, the stationary-phase area increases as frequency decreases; therefore, more sources can contribute to retrieval of the low frequency Green's function. However, the integrand of cross-correlations (eqs 4, 6 and 8) oscillates slower as frequency decreases (Fig. 3). Therefore, if the sources only exist in some small part of the non-stationary-phase area, frequency-dependent energy will remain after the integration and lead to spurious waves (i.e. artefacts) in the retrieved G_{ZZ} (e.g. Yang & Ritzwoller 2008). In contrast, at high frequencies the integrand oscillates rapidly (Fig. 3), and the non-stationary-phase source energy cancels over small angular ranges (Xu *et al.* 2017). If we consider the integrands of C_{ZR} and C_{RR} (Figs 2b and c, respectively), we

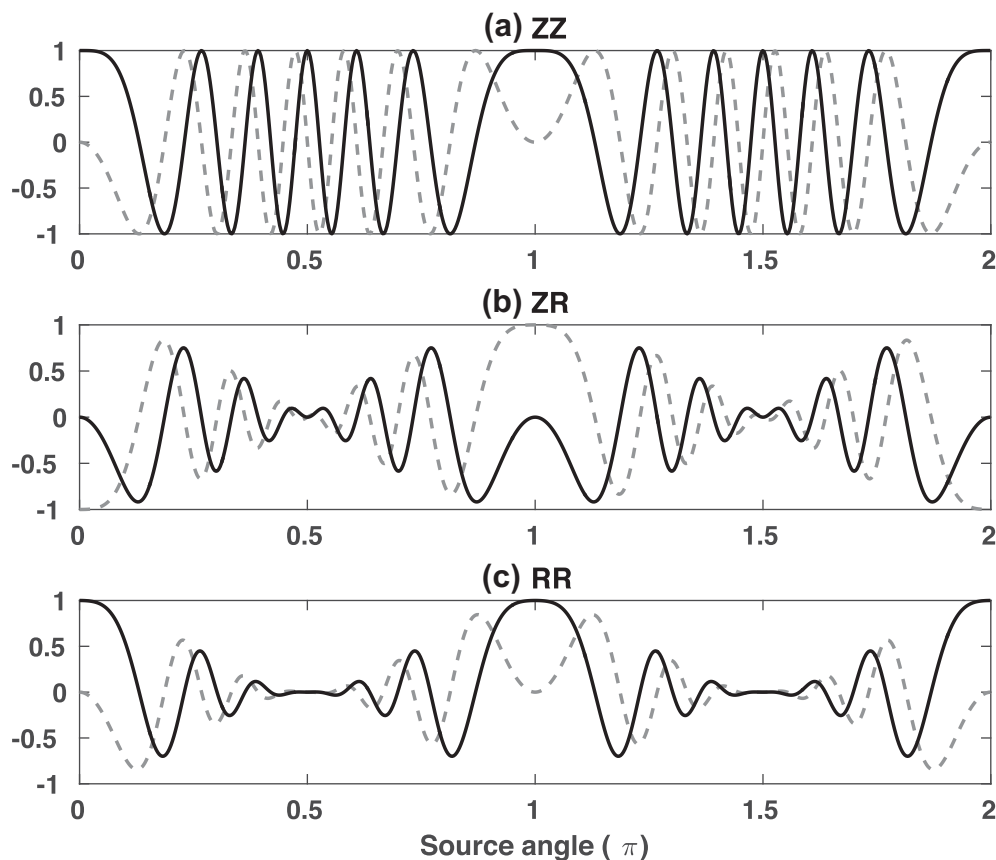


Figure 2. The amplitudes of the integrands of C_{ZZ} , C_{ZR} and C_{RR} (eqs 4, 6 and 8) change with the source angle (θ). The black solid line represents the real part of the integrand, and the grey dashed line represents the imaginary part. These examples are computed with a frequency (ω) of 5 Hz, a phase velocity (c) of 200 m s^{-1} and an interstation distance (r) of 120 m.

observe an interesting relationship between source angle and the amplitude of the integrand.

The non-stationary-phase sources are spatially down weighted in the C_{ZR} and C_{RR} cross-correlations due to the occurrence of the $\cos \theta$ in eqs (6) and (8). For each source, the Rayleigh-wave energy is projected to the R direction and decreases from the maximum to 0 as the source angle increases from $\theta = 0$ to $\pi/2$. Therefore the integrand amplitude of C_{ZR} and C_{RR} is reduced in the non-stationary-phase area compared to the amplitude of C_{ZZ} (Fig. 2). Furthermore, the C_{RR} amplitudes are down weighted more than C_{ZR} outside the stationary-phase area due to the $\cos^2 \theta$ term. Because of the projection in the R direction, C_{RR} is theoretically the most robust Rayleigh-wave estimation for uneven source distributions. Haney *et al.* (2012) pointed out that the $\cos \theta$ term acts as a spatial filter for the C_{ZR} and C_{RR} components in the spatial autocorrelation (SPAC) method. The idea of the spatial filter does not only apply to C_{ZR} , but also to C_{RR} (Fig. 2).

The envelopes of the integrands also demonstrate that C_{ZR} and C_{RR} attenuate the non-stationary-phase energy equally for all frequencies (Fig. 3). The stationary-phase energy in C_{RR} and C_{ZR} is preferentially weighted more than the non-stationary-phase energy, and thus act as a spatial filter on the source distribution. This spatial filter is identical for different frequencies (Fig. 3), different interstation distances and different phase velocities because $\cos \theta$ is independent of these parameters. Furthermore, the filter does not affect the stationary-phase sources because $\cos \theta$ and $\cos^2 \theta$ vary slower than the integrand (Fig. 3). Finally, in the limit that the frequency goes to zero, or the interstation distance goes to zero,

the correlation function becomes an autocorrelation, and all space becomes the stationary-phase area. In that case, the spatial filter no longer plays a significant role in the accuracy of the retrieved Green's function.

4 A SYNTHETIC-NOISE SOURCE EXAMPLE

The integral on the right hand side of eq. (1) also represents the cross-correlation between noise records of two receivers, r_A and r_B , if the noise sources are independent of each other (i.e. mutually uncorrelated) (Wapenaar & Fokkema 2006). One can then use eq. (1) to estimate the Rayleigh-wave Green's functions G_{ZZ} , G_{ZR} and G_{RR} from seismic noise (e.g. Halliday & Curtis 2008). We demonstrate the reliability of C_{ZZ} , C_{ZR} and C_{RR} with a synthetic example, where noise sources are unevenly distributed. We compute virtual shot records along a linear array from correlations of the noise. The noise sources are randomly distributed within two angle ranges (Fig. 4): from $-\pi/12$ to $\pi/12$ (the stationary-phase area) and from $\pi/4$ to $5\pi/12$ (the non-stationary-phase area). The number of noise sources is used as a proxy for the noise energy strength, and the non-stationary-phase noise energy is twice as strong as the stationary-phase noise energy in this example.

The Earth model we use has two layers (Table 1) and is from Bonnefoy-Claudet *et al.* (2006). All noise sources emit the same wavelet, and we model only the fundamental-mode Rayleigh wave. Each noise source is randomly activated during a 1 hr recording

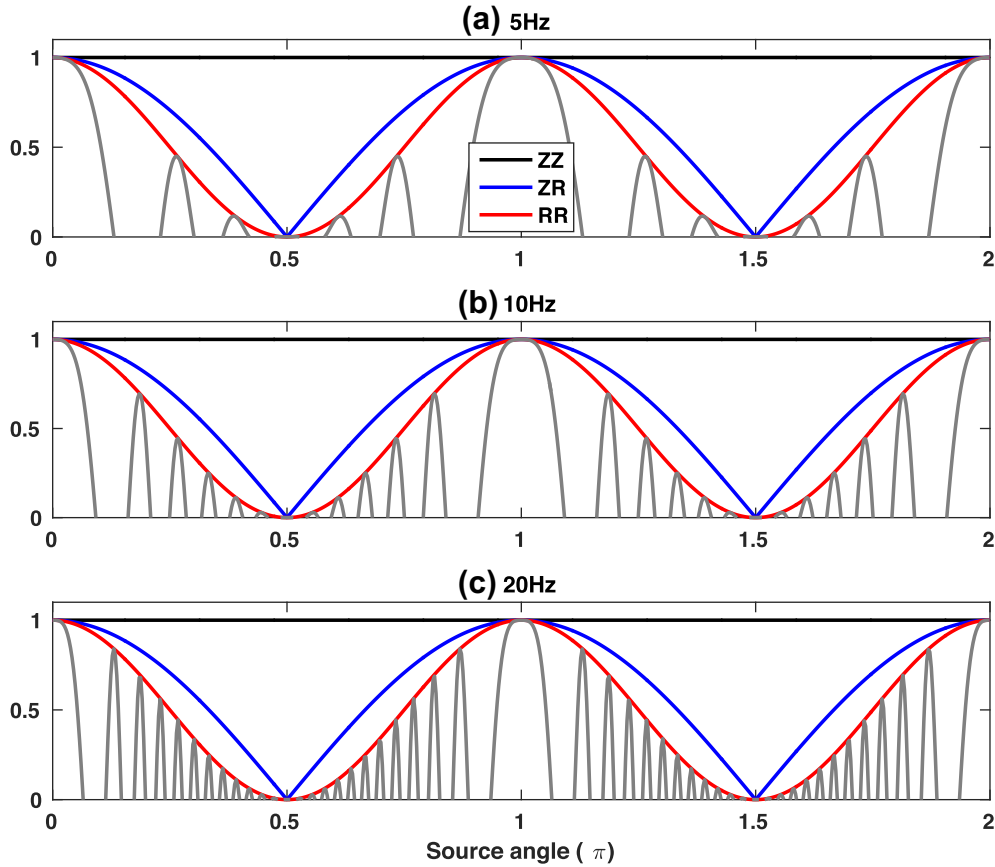


Figure 3. The envelope of the integrand of C_{ZZ} (black line), C_{ZR} (blue line) and C_{RR} (red line) at 5 Hz (a), 10 Hz (b) and 20 Hz (c). The envelope is the L_2 norm of the real and imaginary part of the integrands in eqs (4), (6) and (8). The grey line is the real part of the integrand of C_{RR} weighted by $\cos^2\theta$. The oscillation rate of the phase of C_{ZZ} and C_{ZR} is identical to C_{RR} , and the phase varies much faster than the weighting term. Here we assume the phase velocity is 200 m s^{-1} and the interstation distance is 120 m.

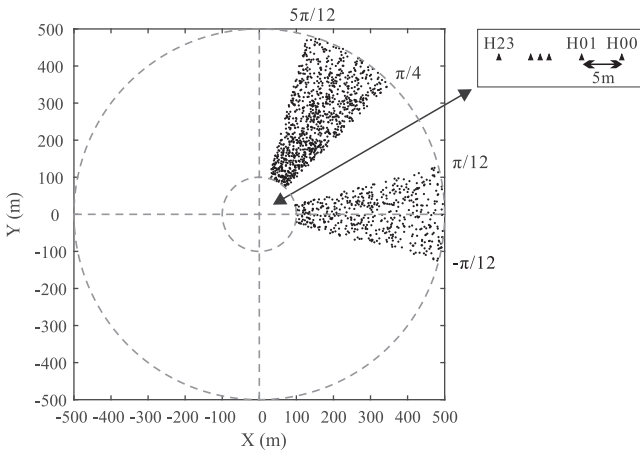


Figure 4. The experiment geometry indicates the location of noise sources (dots) and geophones (triangles). The noise sources are located away from the origin between 100 and 500 m. See the text for more details.

time. We simulate the response for every source using the algorithm proposed by Michaels & Smith (1997) and project the response to the Z and R components of the sensors. Then we stack all of these source projections to create a 1 hr long synthetic noise recording at each of the 24 geophones, which are 5 m apart from each other (Fig. 4), with H13 near the origin.

Table 1. The two-layer Earth model parameters used in the simulation.

Layer number	Vp (m s ⁻¹)	Vs (m s ⁻¹)	Density (kg m ⁻³)	Thickness (m)
1	1350	200	1900	25
2	2000	1000	2500	∞

We assess the accuracy of the three cross-correlations by comparing virtual shot records and comparing the Rayleigh-wave phase-velocity dispersion images to the true dispersion. We build virtual shot records (Figs 5a–c) from individual cross-correlations (e.g. Halliday *et al.* 2008) and then map the data to the frequency-velocity domain using the phase-shift method (Song *et al.* 1989) to generate phase-velocity dispersion images (Figs 5d–f). The virtual shot records and the dispersion images indicate that C_{RR} is the most robust among the three cross-correlations. The dominate waveforms in the three cross-correlations are from the stationary-phase area noise sources, and the high-velocity spurious wave before the main waveform is due to the non-stationary-phase area noise energy. We find that C_{RR} contains lower-amplitude spurious waves than C_{ZR} and C_{ZZ} (Fig. 6). The spurious waves in C_{ZZ} lead to the spurious energy trends at frequencies less than 7 Hz (Fig. 5d), which is fully discussed in Xu *et al.* (2017). We also find that C_{ZR} does not provide accurate information below 5 Hz (Fig. 5e). However, we observe accurate Rayleigh-wave phase velocities in the frequency-velocity domain of the C_{RR} below 5 Hz (Fig. 5f), which matches the theoretical prediction in Section 3.

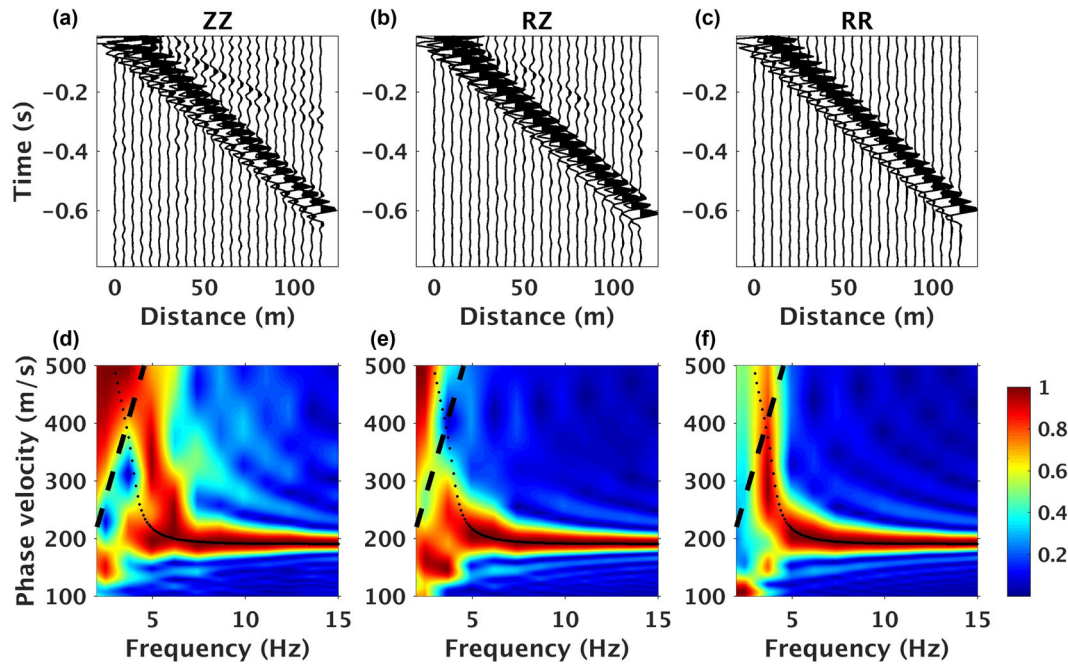


Figure 5. C_{ZZ} , C_{RZ} and C_{RR} virtual shot records (a–c) and the corresponding phase-velocity dispersion images (d–f). The dominant energy trends in (a–c) represent the Rayleigh wave. Black dots represent theoretical Rayleigh-wave phase velocities (Haskell 1953) in (d–f). The black dash lines in (d–f) indicate the resolvable image area, where the wavelength is less than the array length. All dispersion images are normalized per frequency.

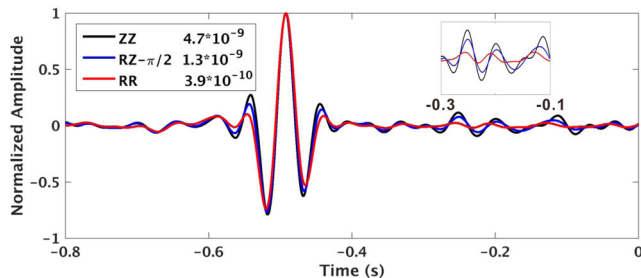


Figure 6. The amplitude normalized C_{ZZ} , C_{RZ} and C_{RR} functions between receivers H00 and H20. The inset shows a zoom of the spurious-energy time window from -0.1 to -0.3 s. A $\pi/2$ phase shift has been applied to C_{RZ} to facilitate the comparison with C_{ZZ} and C_{RR} . The values in the legend indicate the maximum amplitude of each cross-correlation function.

5 DISCUSSION

Although C_{ZR} and C_{RR} attenuate non-stationary sources, the amplitudes of these two cross-correlations are determined by the H/V ratio (eqs 6 and 8). The H/V ratio is normally less than 1; therefore, the C_{ZZ} amplitude is normally larger than C_{ZR} and C_{RR} . In our synthetic data example, the 3–15 Hz frequency-averaged H/V ratio is 0.41, the standard deviation is 0.21, and the C_{RR} peak amplitude is an order of magnitude smaller than the C_{ZZ} peak amplitude (Fig. 6). Relative to the maximum amplitude of each correlation, the coherent noise (Fig. 6, $t > -0.4$ s and inset) is much larger in C_{ZZ} than C_{RR} , while the incoherent noise (Fig. 6, $t < -0.6$ s) is approximately the same. Therefore, when discussing notions of SNR, one needs to consider both coherent and incoherent noise. Artefacts due to an uneven source distribution should be considered coherent noise, while random fluctuations should be considered incoherent noise.

In most studies, authors compute SNR as the ratio between the maximum Rayleigh-wave amplitude and the incoherent noise (e.g. Bensen *et al.* 2007; Lin *et al.* 2008). The incoherent noise is measured based on a window of data after the direct arrival (e.g. Bensen

et al. 2007; Lin *et al.* 2008). If we assume that the random fluctuation (i.e. incoherent noise) amplitude is the same on the Z component and the R component, then the SNR of C_{ZR} and C_{RR} will be less than that of C_{ZZ} any time the Rayleigh wave H/V ratio is less than 1. Thus in practice, people observe (compute) that C_{ZZ} has a higher SNR than C_{ZR} and C_{RR} (e.g. Lin *et al.* 2008). However, this SNR metric does not take into account the coherent noise that precedes the direct Rayleigh wave. One approach to monitor the coherent noise is to use a continuous SNR computation method (e.g. Larose *et al.* 2007; Clarke *et al.* 2011).

Finally, C_{ZR} and C_{RR} can also aid the identification of fundamental and higher-mode surface waves when the two surface-wave dispersion curves are very close in the frequency-velocity domain (Boué *et al.* 2016; Ma *et al.* 2016). The fact that Rayleigh wave modes have different H/V ratios and particle motions enables one to identify (e.g. Boaga *et al.* 2013) and separate these modes (e.g. Gribler *et al.* 2016) to improve the reliability of dispersion estimation.

6 CONCLUSIONS

We present the relationships between the fundamental-mode Green's functions (G_{ZZ} , G_{ZR} and G_{RR}) and cross-correlation functions (C_{ZZ} , C_{ZR} and C_{RR}) within the far-filed approximation. When estimating the fundamental-mode Rayleigh-wave Green's functions, the C_{ZZ} cross-correlation weights source energy equally from all directions. In contrast, the C_{ZR} and C_{RR} cross-correlations attenuate source energy in the non-stationary-phase area for all frequencies and thus act as spatial filters on the source distribution. Therefore, more accurate Green's functions (i.e. fewer spurious arrivals or reduced coherent noise) are retrieved from C_{ZR} and C_{RR} compared to C_{ZZ} when the source energy is unevenly distributed. We demonstrate the validity of this theoretical inference with a synthetic seismic noise example. Those interested in characterizing velocity structure from ambient noise Rayleigh waves should use C_{RR} whenever possible to limit the effect of non-homogeneous

noise source distributions on the frequency-dependent direct-wave phase velocity. Finally, we note that the analysis presented here pertains to the direct-wave Rayleigh wave; we have neglected how the multicomponent cross-correlations influence scattered waves.

REFERENCES

- Baig, A.M., Campillo, M. & Brenguier, F., 2009. Denoising Seismic noise cross correlations, *J. geophys. Res.*, **114**(8), 1–12.
- Bensen, G.D., Ritzwoller, M.H., Barmin, M.P., Levshin, A.L., Lin, F., Moschetti, M.P. & Yang, Y., 2007. Processing seismic ambient noise data to obtain reliable broad-band surface wave dispersion measurements, *Geophys. J. Int.*, **169**(3), 1239–1260.
- Boaga, J., Cassiani, G., Strobbia, C.L. & Vignoli, G., 2013. Mode misidentification in Rayleigh waves: ellipticity as a cause and a cure, *Geophysics*, **78**(4), EN17–EN28.
- Bonnefoy-Claudet, S., Cornou, C., Bard, P.Y., Cotton, F., Moczo, P., Kristek, J. & Fäh, D., 2006. H/V ratio: a tool for site effects evaluation. Results from 1-D noise simulations, *Geophys. J. Int.*, **167**(2), 827–837.
- Boué, P., Denolle, M., Hirata, N., Nakagawa, S. & Beroza, G.C., 2016. Beyond basin resonance: characterizing wave propagation using a dense array and the ambient seismic field, *Geophys. J. Int.*, **206**(2), 1261–1272.
- Campillo, M. & Paul, A., 2003. Long-range correlations in the diffuse seismic coda, *Science*, **299**(5606), 547–549.
- Clarke, D., Zaccarelli, L., Shapiro, N.M. & Brenguier, F., 2011. Assessment of resolution and accuracy of the Moving Window Cross Spectral technique for monitoring crustal temporal variations using ambient seismic noise, *Geophys. J. Int.*, **186**(2), 867–882.
- Fan, Y. & Snieder, R., 2009. Required source distribution for interferometry of waves and diffusive fields, *Geophys. J. Int.*, **179**(2), 1232–1244.
- Froment, B., Campillo, M., Roux, P., Gouédard, P., Verdel, A. & Weaver, R.L., 2010. Estimation of the effect of nonisotropically distributed energy on the apparent arrival time in correlations, *Geophysics*, **75**(5), SA85–SA93.
- Froment, B., Campillo, M. & Roux, P., 2011. Reconstructing the Green's function through iteration of correlations, *C. R. Geosci.*, **343**(8–9), 623–632.
- Gribler, G., Liberty, L.M., Mikesell, T.D. & Michaels, P., 2016. Isolating retrograde and prograde Rayleigh-wave modes using a polarity mute, *Geophysics*, **81**(5), V379–V385.
- Halliday, D. & Curtis, A., 2008. Seismic interferometry, surface waves and source distribution, *Geophys. J. Int.*, **175**(3), 1067–1087.
- Halliday, D., Curtis, A. & Kragh, E., 2008. Seismic surface waves in a suburban environment: active and passive interferometric methods, *Leading Edge*, **7**(2), 210–218.
- Haney, M.M., Mikesell, T.D., van Wijk, K. & Nakahara, H., 2012. Extension of the spatial autocorrelation (SPAC) method to mixed-component correlations of surface waves, *Geophys. J. Int.*, **191**(1), 189–206.
- Haskell, N.A., 1953. The dispersion of surface waves on multilayered media, *Bull. seism. Soc. Am.*, **43**(1), 17–34.
- Larose, E., Roux, P. & Campillo, M., 2007. Reconstruction of Rayleigh-Lamb dispersion spectrum based on noise obtained from an air-jet forcing, *J. acoust. Soc. Am.*, **122**(6), 3437–3444.
- Lin, F., Moschetti, M.P. & Ritzwoller, M.H., 2008. Surface wave tomography of the western United States from ambient seismic noise: Rayleigh and Love wave phase velocity maps, *Geophys. J. Int.*, **173**(1), 281–298.
- Lobkis, O.I. & Weaver, R.L., 2001. On the emergence of the Green's function in the correlations of a diffuse field, *J. acoust. Soc. Am.*, **110**(6), 3011–3017.
- Ma, Y., Clayton, R.W. & Li, D., 2016. Higher-mode ambient-noise Rayleigh waves in sedimentary basins, *Geophys. J. Int.*, **206**(3), 1634–1644.
- Melo, G., Malcolm, A., Mikesell, T.D. & van Wijk, K., 2013. Using SVD for improved interferometric green's function retrieval, *Geophys. J. Int.*, **194**(3), 1596–1612.
- Michaels, P. & Smith, R., 1997. Surface wave inversion by neural networks (radial basis functions) for engineering applications, *J. Environ. Eng. Geophys.*, **2**(1), 65–76.
- Mikesell, T.D., van Wijk, K., Calvert, A. & Haney, M.M., 2009. The virtual refraction: useful spurious energy in seismic interferometry, *Geophysics*, **74**(3), A13–A17.
- Mikesell, T.D., van Wijk, K., Blum, T.E., Snieder, R. & Sato, H., 2012. Analyzing the coda from correlating scattered surface waves, *J. acoust. Soc. Am.*, **131**, EL275, doi:10.1121/1.3687427.
- Mulargia, F., 2012. The seismic noise wavefield is not diffuse, *J. acoust. Soc. Am.*, **131**(4), 2853–2858.
- Nakata, N., Chang, J.P., Lawrence, J.F. & Boué, P., 2015. Body wave extraction and tomography at Long Beach, California, with ambient-noise interferometry, *J. geophys. Res.*, **120**(2), 1159–1173.
- Nishida, K., Kawakatsu, H., Fukao, Y. & Obara, K., 2008. Background Love and Rayleigh waves simultaneously generated at the Pacific Ocean floors, *Geophys. Res. Lett.*, **35**, L16307, doi:10.1029/2008GL034753.
- Roux, P., Sabra, K.G., Kuperman, W.A. & Roux, A., 2005. Ambient noise cross correlation in free space: Theoretical approach, *The J. acoust. Soc. Am.*, **117**(1), 79–84.
- Shapiro, N.M., Michel, C., Laurent, S. & Ritzwoller, M.H., 2005. High-resolution surface-wave tomography from ambient seismic noise, *Science*, **307**, 1615–1618.
- Snieder, R., 2004. Extracting the Green's function from the correlation of coda waves: a derivation based on stationary phase, *Phys. Rev. E*, **69**(4), 046610, doi:10.1103/PhysRevE.69.046610.
- Snieder, R., Wapenaar, K. & Larner, K., 2006. Spurious multiples in seismic interferometry of primaries, *Geophysics*, **71**(4), S1111–S1124.
- Snieder, R., Van Wijk, K., Haney, M. & Calvert, R., 2008. Cancellation of spurious arrivals in Green's function extraction and the generalized optical theorem, *Phys. Rev. E*, **78**(3), 1–8.
- Song, Y., Castagna, J.P., Black, R.A. & Knapp, R.W., 1989. Sensitivity of near-surface shear-wave velocity determination from Rayleigh and Love waves, in *SEG, 59th Annual Meeting*, Dallas, Texas, pp. 509–512.
- Stehly, L., Campillo, M., Froment, B. & Weaver, R.L., 2008. Reconstructing Green's function by correlation of the coda of the correlation (C^3) of ambient seismic noise, *J. geophys. Res.*, **113**, B11306, doi:10.1029/2008JB005693.
- Stehly, L., Fry, B., Campillo, M., Shapiro, N.M., Guilbert, J., Boschi, L. & Giardini, D., 2009. Tomography of the Alpine region from observations of seismic ambient noise, *Geophys. J. Int.*, **178**(1), 338–350.
- Stehly, L., Cupillard, P. & Romanowicz, B., 2011. Towards improving ambient noise tomography using simultaneously curvelet denoising filters and SEM simulations of seismic ambient noise, *C. R. Geosci.*, **343**(8–9), 591–599.
- van Wijk, K., Mikesell, T.D., Schulte-Pelkum, V. & Stachnik, J., 2011. Estimating the Rayleigh-wave impulse response between seismic stations with the cross terms of the Green tensor, *Geophys. Res. Lett.*, **38**, L16301, doi:10.1029/2011GL047442.
- Wapenaar, K. & Fokkema, J., 2006. Green's function representations for seismic interferometry, *Geophysics*, **71**(4), S133–S146.
- Wapenaar, K., Ruigrok, E., Van Der Neut, J. & Draganov, D., 2011. Improved surface-wave retrieval from ambient seismic noise by multi-dimensional deconvolution, *Geophys. Res. Lett.*, **38**(1), 1–5.
- Weaver, R.L. & Lobkis, O.I., 2006. Diffuse fields in ultrasonics and seismology, *Geophysics*, **71**(4), S15–S19.
- Xu, Z., Mikesell, T.D., Xia, J. & Cheng, F., 2017. A comprehensive comparison between the refraction microtremor and seismic interferometry method for phase velocity estimation, *Geophysics*, in review.
- Yang, Y. & Ritzwoller, M.H., 2008. Characteristics of ambient seismic noise as a source for surface wave tomography, *Geochem. Geophys. Geosyst.*, **9**(2), 1256–1256.
- Yao, H. & van Der Hilst, R.D., 2009. Analysis of ambient noise energy distribution and phase velocity bias in ambient noise tomography, with application to SE Tibet, *Geophys. J. Int.*, **179**(2), 1113–1132.